Development and Evaluation of selective nitroxanthone Derivatives: A promising compound for Targeting MCF-7 breast cancer cells

Pavithren Devakrishnan [a], Nadiah Mad Nasir [a,*], Johnson Stanslas [b], Muhammad Alif M. Latif [c], Ahmad Zaidi Ismail [a], Fatin Farhana Baharuddin [a]

[a] Department of Chemistry, Faculty of Sciences, University Putra Malaysia, Serdang, Selangor 43400 Malaysia
[b] Department of Medicine, Faculty of Medicine and Health Sciences, Universiti Putra Malaysia, Serdang, Selangor 43400 Malaysia
[c] Centre of Foundation Studies for Agricultural Science, University Putra Malaysia, Serdang, Selangor 43400 Malaysia

ARTICLE INFO

ABSTRACT

A series of nitroxanthone derivatives (1–6) were synthesized and evaluated for their potential efficacy against estrogen-receptor positive (MCF-7) and triple-negative breast cancer cell lines (MDA-MB-231). Cell viability assays identified compound 1 at 10 μM as the most promising candidate due to its potent growth inhibitory activity (22.05 ± 2.40 %) against the MCF-7 cell line. The half-maximal inhibitory concentration (IC_{50}) of compound 1 was 7.00 ± 0.00 μM for MCF-7 cells, compared to 250.00 ± 70.71 μM for HaCaT and 800.00 ± 0.00 μM for RAW 264.7 cells, yielding selectivity indices (SI) of 35.71 and 114.29, respectively. Additionally, compound 1 exhibited mortality concentrations of 1736.58 μM and 3660.35 μM for zebrafish and brine shrimp embryos, with SI values of 522.91 and 248.08, respectively. Molecular docking analysis showed that compound 1 binds more efficiently to the target enzyme aromatase compared to other derivatives, likely due to its optimal number of nitro groups, orientations, and polarizabilities. Crystal structure analysis revealed that compound 1 crystallizes in the monoclinic system with the C2/c space group. In summary, compound 1 demonstrates selective toxicity towards tumor cells (MCF-7) while being non-toxic to normal cell lines (HaCaT and RAW 264.7) and in vivo studies with brine shrimp and zebrafish. These findings suggest that compound 1 holds promise as a lead compound to target breast cancer cells.

1. Introduction

Breast cancer remains a significant public health concern, with many countries experiencing escalating incidence rates. Despite current preventative efforts, the illness is expected to become more prevalent over the next two decades. This trend is associated with the increased number of women harboring major risk factors for breast cancer worldwide, such as early menarche, late first pregnancies, fewer pregnancies, shorter or no lactation periods, and late menopause [1,2]. Approximately 2.3 million women were identified with breast cancer in 2022, and 670,000 died worldwide [3]. Although breast cancer impacts women of all ages after puberty, its prevalence intensifies later in life. Global assessments of breast cancer burden indicate notable discrepancies predicated on human development. For instance, 1 in every 12 women in nations with a high Human Development Index (HDI) is anticipated to be diagnosed with breast cancer at some point in her life, and 1 in every 71 will die from this condition [4]. Aromatase is prominent in the biosynthesis of estrogen, a vital hormone in many physiological processes, especially in females. It is responsible for the conversion of androgens, such as testosterone and androstenedione, into estrogen, including estradiol

Table 1
Commonly used anti-breast cancer drugs and associated side effects.

Type of Therapies	Anti-Breast Cancer Drugs	Side Effects
Hormonal Therapies	Tamoxifen [13]	Hot flashes, vaginal dryness, mood swings, blood clots, increased risk of uterine cancer
Targeted Therapies	Anastrozole [14] Letrozole [15] Exemestane [16]	Joint pain, bone loss (osteoporosis), fatigue, hot flashes
	Trastuzumab (Herceptin) [17]	Heart damage, infusion reactions, fatigue, nausea
	Pertuzumab [18]	Diarrhea, infusion reactions, heart dysfunction
	Palbociclib [19] Ribociclib [20] Abemaciclib [21]	Low white blood cell counts, nausea, fatigue, diarrhea
Chemotherapy	Olaparib [22] Talazoparib [23]	Nausea, anemia, fatigue, low blood cell counts
	Doxorubicin (Adriamycin) [24]	Hair loss, nausea, heart damage, fatigue
	Paclitaxel [25] Docetaxel [26]	Hair loss, peripheral neuropathy, allergic reactions, low blood counts
	Cyclophosphamide [27]	Nausea, bladder irritation, low white blood cells, hair thinning
Immunotherapy	Atezolizumab [28]	Fatigue, rash, diarrhea, inflammation of organs (such as lungs, liver)
Bone-modifying Agents	Zoledronic Acid [29]	Fever, myalgia, fatigue and influenza-like
	Denosumab [30]	Bone pain, low calcium levels, jaw osteonecrosis

(the most potent estrogen) [5]. This conversion occurs primarily in the ovaries, testes, placenta, and adipose (fat) tissues. Its presence in different tissues allows for the localized production of oestrogen [6]. A study reported that although aromatase activity helps maintain normal estrogen levels in the body, aromatase activity dysregulation can cause hormonal abnormalities leading to various health consequences, including breast cancer [7].

Many medications have been discovered for breast cancer patients. However, most of them are toxic and adversely affect normal cells and tissues as described in Table 1. Consequently, researchers are now motivated to further develop innovative medications for cancer therapy with better selectivity towards tumor cells and without adverse effects on normal cells [8]. Xanthone is a group of naturally occurring organic compounds that have garnered considerable interest in the fields of chemistry, pharmacology, and medicine due to their diverse range of biological activities and potential therapeutic applications [9]. It is a group of oxygenated heterocyclic compounds characterized by a tricyclic structure consisting of two benzene rings fused to a central six-membered ring. Xanthones are known as "privileged structures" because they can bind to several receptors and, as a result, demonstrate potent pharmacological effects against various disorders [10]. As a consequence, xanthones have piqued the interest of researchers and pharmaceutical scientists as drug candidates and health-promoting medicines. Different substituents exhibit a wide range of pharmacological activities, and previous research reported that xanthones with oxygen substituents could enhance anticancer activity [11]. In 2018, Zhou group had patented a nitroxanthone derivative with inhibitory effect on human liver cancer SMMC-7721 cells and human cervical cancer Hela cells, the cell inhibition rates are 90.17 ± 0.41 % and 51.20 ± 0.37 %, respectively, and the IC$_{50}$ is 14.02 ± 0, and 36.55 ± 0.69 μm, respectively [12]. These results showed that nitroxathone is highly potent against cancer cell lines. Hence, our group is interested in investigating the nitroxanthone derivatives with different positions of the nitro group against MCF-7 cell lines. Indirectly, the aromatase is a protein of MCF-7 cells.

In this study, we focus on the nitro compounds which have demonstrated great importance in long-standing studies of their utilization in synthetic organic chemistry, the nitro compounds have been considered promising compounds against diverse diseases [31], as well as, they have been present in several approved drugs such as nilutamide (non-steroidal antiandrogen) [32], nitrendipine (Alzheimer's disease) [33] and nitrazepam (anticonvulsant) [34].

The nitro group (NO$_2$) is a functional group formed by one nitrogen atom linked to two oxygens, it is a particularly electron-withdrawing moiety since the N has no lone pair, hence it bears a positive charge [35]. The electron-withdrawing group (EWG) effect is observed in aromatic rings due to resonance with the nitro group, which deactivates certain positions and alters the molecule's polarity. This change can enhance interactions with nucleophilic sites in protein structures, such as enzymes, potentially leading to inhibition [36]. Another study about the electron-donating group (EDG) by the Lee group [37] reported *o*-OCH$_3$ (alkyl group) is an excellent substituent for designing potent antioxidants with increasing the number of *o*-OCH$_3$ groups on the phenol ring further enhances the antioxidant activity.

Inspired by previous research on xanthone derivatives, we aimed to expand the range of nitroxanthone derivatives (**1–6**) by synthesizing them using a modified method of Grover, Shah, and Shah, with substitutions at the *ortho*, *meta*, and *para* positions as in Fig. 1 [38,39]. Their anti-breast cancer activities were evaluated on human breast cancer cell lines (MCF-7 and MDA-MB-231) using a tetrazolium-based (MTT) assay. This study also investigates how the position of nitro groups and addition of alkyl group affects their activity based on the structure activity relationship (SAR). Additionally, the cytotoxicity of the most potent compound was evaluated both *in vitro* and *in vivo*. The results confirm the potential of nitroxanthones for development into valuable healthcare products and applications.
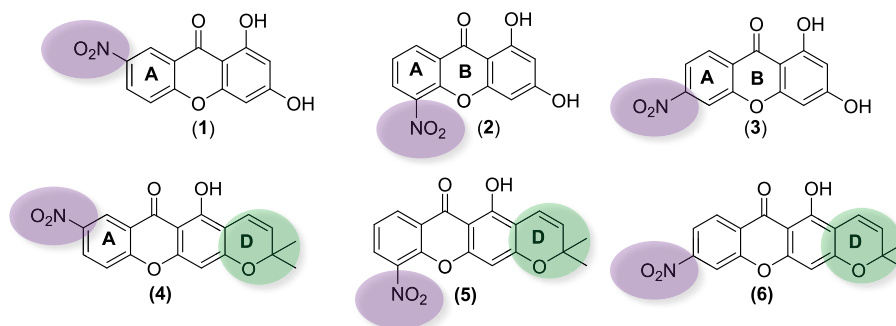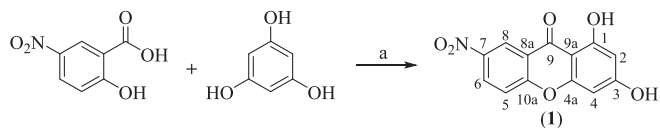

Fig. 1. *Ortho*, *meta* and *para* nitroxanthone at ring A and alkylation at ring D.

Scheme 1. The synthesis of xanthone derivatives: (a) Eaton's reagent, reflux 20 min, 80 °C.

2. Experimental section

2.1. Chemistry

The reactions in this study were conducted under a nitrogen atmosphere using reagents acquired from commercial suppliers, such as Sigma-Aldrich, Merck, and Alfa Aesar. The crude products were purified using column chromatography on Sigma-Aldrich silica gel with a 100–200 mesh size. Thin-layer chromatography (TLC) plates were visualised using ultraviolet light at 254 and 365 nm for short and long waves. The 1D and 2D NMR spectra (^{1}H, ^{13}C, HSQC, and HMBC) were obtained by VARIAN 500 MHz and recorded in deuterated solvents at 500 MHz (^{1}H) and 125 MHz (^{13}C), with chemical shifts reported in parts per million (ppm) relative to TMS. Mass spectra were obtained using direct-injection (DIMS) techniques, and infrared spectra (IR) were obtained using the Attenuated Total Reflectance (ATR) technique. Melting points were obtained using a Fisher-Johns melting point apparatus.

2.2. Experimental synthesis of nitro xanthone derivative

The nitro xanthone derivatives **1**–**3** were prepared using the modified Grover, Shah, and Shah reaction [40]. Eaton's reagent (4.00 mL) was slowly added to react with the mixture of salicylic acid derivatives (5.46 mmol/1.00 g) and phloroglucinol (5.46 mmol/0.69 g). The mixture was refluxed for 20 min at 80 °C in an oil bath with constant stirring. After the reaction, the product was cooled at room temperature and cold distilled water was added and stirred for one hour in an ice water bath. The formed precipitate was filtered, rinsed with cold distilled water, and dried overnight. The crude products underwent additional purification using column chromatography on silica gel to obtain the desired xanthone derivative. Then, to synthesize nitro xanthone derivatives (**4**–**6**) from derivatives of **1**–**3**, 3-methyl-2-butenal (3 mmol) was added to a solution of the derivatives (**1**–**3**), (1 mmol) and calcium hydroxide, Ca(OH)$_2$ (2 mmol), in methanol [40,41]. The resulting solution was stirred for 36 h at room temperature. Upon completion of the reaction, the reaction mixture was then diluted with ethyl acetate, followed by extraction and washing with 2 M hydrochloric acid (HCl), water, and brine. The resulting product was then dried over anhydrous MgSO$_4$ and concentrated under vacuum. The crude products were subjected to column chromatography for further purification.

2.2.1. Structural elucidation and characterization of nitro xanthone derivative

2.2.1.1. Synthesis of 7-nitro-1,3-dihydroxy-9H-xanthen-9-one (1).. Dark yellow solid; yield 78 %; m.p 277.30 °C; [Eluent: Hexane: Ethyl acetate (9:1)]; ^{1}H NMR (500 MHz, DMSO-d_6) δ: 4.95 (2H, s, 1-OH & 3-OH), 6.29 (1H, d, $J = 1.95$ Hz, H-4), 6.48 (1H, d, $J = 1.95$ Hz, H-2), 7.83 (1H, d, $J = 9.25$, H-5), 8.60 (1H, dd, $J = 2.75, 9.25$ Hz, H-6), 8.80 (1H, d, $J = 2.75$ Hz, H-8), 12.40 (2H, s, 1-OH & 3-OH); ^{13}C NMR (125 MHz, DMSO-d_6) δ: 94.40, 98.64, 117.73, 119.12, 121.42, 126.38, 128.92, 129.45, 129.45 159.12, 163.64, 166.86, 178.85; IR (ATR) 3337.00 (OH), 2359.00 (CH aromatic), 1620.00 (C = O), 1511.00 (NO), 1528.00 (C = C aromatic), 1265.00 (CN), 1216.00 (CO) cm^{-1}; DI-MS m/z calcd for C$_{13}$H$_7$NO$_6$ [M]$^+$ 273.20, found 273.05 [42]

2.2.1.2. Synthesis of 5-nitro-1,3-dihydroxy-9H-xanthen-9-one (2).. Dark yellow solid; yield 40.54 %; m.p 270.20 °C; [Eluent: Hexane: Ethyl acetate (9:1)]; ^{1}H NMR (500 MHz, methanol-d_4) δ: 4.00 (1H, s, 3-OH), 4.60 (1H, s, 1-OH), 6.26 (1H, d, $J = 2.1$ Hz, H-4), 6.41 (1H, d, $J = 2.1$ Hz, H-2), 7.55 (1H, dd, $J = 7.9, 7.9$ Hz, H-7), 8.39 (1H, dd, $J = 1.6, 7.9$ Hz, H-8), 8.50 (1H, dd, $J = 1.6, 7.9$ Hz, H-6); ^{13}C NMR (125 MHz, methanol-d_4) δ: 94.43, 98.82, 122.97, 105.41, 109.99, 130.26, 130.53, 161.95, 155.54, 155.89, 162.97, 164.46, 178.29; IR (ATR) 3347.54

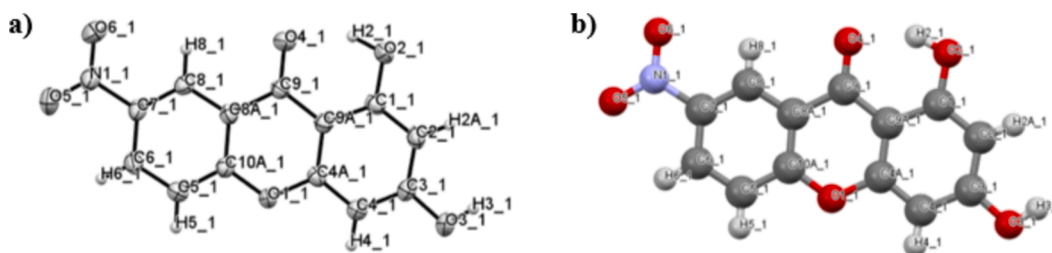
Fig. 2. The molecular structure of 1; a) ORTEP with the atom-labelling scheme and 50% probability ellipsoids; b) optimized structure.
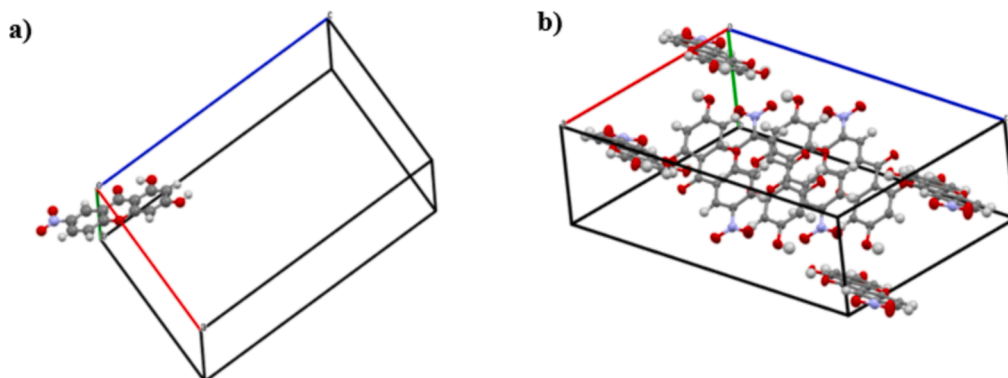

Fig. 3. The arrangement of 1; a) The asymmetric unit; b) The unit cell that contains eight molecules.

Table 2

Experimental details for 7-nitro-1,3-dihydroxy-9H-xanthen-9-one (1).

Crystal Data	7-nitro-1,3-dihydroxy-9H-xanthen-9-one (1)
Chemical formula	$C_{13}H_7NO_6$
M_r	273.20
Crystal system, space group	Monoclinic, C2/c
Temperature (K)	301
a, b, c (Å)	14.265 (3), 7.0591 (15), 21.712 (4)
β (°)	98.103 (7)
V (Å³)	2164.5 (7)
Z	8
Radiation type	Mo Kα
μ (mm^{-1})	0.14
Crystal size (mm)	0.3 × 0.3 × 0.03
Data collection	
Diffractometer	Bruker APEX-II CCD
Absorption correction	Multi-scan
	SADABS2016/2 (Bruker,2016/2) was used for absorption correction. wR2(int) was 0.0722 before and 0.0642 after correction. The Ratio of minimum to maximum transmission is 0.9421. The λ/2 correction factor is Not present.
T_{min}, T_{max}	0.703, 0.746
No. of measured, independent and observed [I > 2σ(I)] reflections	31891, 2701, 1787
R_{int}	0.101
$(\sin\theta/\lambda)_{max}$ (Å^{-1})	0.667
Refinement	
$R[F^2 > 2\sigma(F^2)], wR(F^2), S$	0.051, 0.125, 1.07
No. of reflections	2701
No. of parameters	187
H-atom treatment	H atoms treated by a mixture of independent and constrained refinement
$\Delta\rho_{max}$, $\Delta\rho_{min}$ (e Å^{-3})	0.26, −0.22

Table 3

Percentage of cell viability for two different breast cancer cell lines (MCF-7 and MDA-MB-231).

Compounds	Concentration (μM)	Cell Viability (%)	
		MCF-7	MDA-MB-231
1	10	22.05 ± 2.40	98.92 ± 2.76
2	10	93.49 ± 1.64	97.94 ± 1.78
3	10	93.42 ± 2.36	99.80 ± 3.00
4	10	107.96 ± 4.78	96.08 ± 0.6
5	10	92.78 ± 5.81	102.16 ± 1.94
6	10	101.01 ± 0.26	110.93 ± 3.10
Gemcitabine	10	22.20 ± 1.95	33.68 ± 1.87

*Gemcitabine = a standard drug.

Table 4

Percentage of cell viability for MCF-7 breast cancer cell line and BEAS-2B normal lung cell line.

Compounds	Concentration (μM)	Cell Viability (%)	
		MCF-7	BEAS-2B
1	10	22.05 ± 2.40	94.15 ± 0.12
Gemcitabine	10	22.20 ± 1.95	9.64 ± 0.50

*Gemcitabine = a standard drug.

(OH), 1976.17 (CH aromatic), 1737.38 (C = O), 1529.94 (NO), 1459.84 (C = C aromatic), 1267.32 (CN), 1090.14 (CO) cm^{-1}; DI-MS m/z calcd for $C_{13}H_7NO_6$ [M]$^+$ 273.00, found 273.00 [42]

2.2.1.3. Synthesis of 6-nitro-1,3-dihydroxy-9H-xanthen-9-one (3).. Light-yellow solid; 37.63 %; m.p 229.20 °C; [Eluent: Hexane: Ethyl acetate (9:1)]; ^{1}H NMR (500 MHz, methanol-d_4) δ: 4.01 (1H, s, 3-OH), 4.97 (1H,

s, 1-OH), 7.70 (1H, s, H-5), 7.72 (1H, d, J = 2.2 Hz, H-4), 7.73 (1H, d, J = 2.2 Hz, H-2), 8.08 (1H, d, J = 8.6 Hz, H-8), 8.09 (1H, d, J = 8.6 Hz, H-7); ^{13}C NMR (125 MHz, methanol-d_4) δ: 94.13, 98.40, 111.74, 112.85, 113.22, 117.85, 117.72, 127.12, 131.61, 151.96, 162.02, 170.66; IR (ATR) 3281.00 (OH), 1955.00 (CH aromatic), 1681.00 (C = O), 1516.00 (NO), 1480.00 (C = C aromatic), 1278.00 (CN), 1172.00 (CO) cm^{-1}; DIMS m/z calcd for $C_{13}H_7NO_6$ [M]$^+$ 273.00, found 273.00

2.2.1.4. Synthesis of 1-hydroxy-3′,3′-dimethyl-7-nitropyrano[3,2–b] xanthen-6(2H)-one (4).. Oily yellow; 49.00 %; [Eluent: Hexane: Ethyl acetate (9:5)]; ^{1}HNMR (500 MHz, acetone-d_6) δ: 1.29 ppm (s, 6H, 2-CH$_3$), 5.83 (d, 1H, J = 10.10 Hz, H-2′), 6.49 (s, 1H, H-4), 6.71 (d, 1H, J = 10.10 Hz, H-1′), 7.22 (d,1H, J = 9.20 Hz, H-5), 8.42 (dd, 1H, J = 2.90, 9.20 Hz, H-6), 8.72 (d, 1H, J = 2.90 Hz, H-8), 11.41 (s, 1H, 1-OH); ^{13}C NMR (125 MHz, acetone-d_6) δ:27.67, 109.99, 112.48, 114.34, 118.56, 119.71, 126.15, 136.08, 141.73, 130.48, 152.40, 153.45, 166.71, 168.97, 174.64, 177.17, 179.79; IR (ATR) 3390 (OH), 2890 (CH alkane), 1855 (CH aromatic), 1681 (C = O), 1625 (C = C aromatic), 1522 (NO), 1342 (CN), 1074 (CO) cm^{-1}; DI-MS m/z calcd for $C_{18}H_{13}NO_6$ [M]$^+$ 339.15 found 339.00

2.2.1.5. Synthesis of 1-hydroxy-3′,3′-dimethyl-5-nitropyrano[3,2–b] xanthen-6(2H)-one (5).. Light yellow solid; 45.00 %; m.p 231.90 °C; [Eluent: Hexane: Ethyl acetate (9:5)]; ^{1}H NMR (500 MHz, methanol-d_4) δ: 1.49 (s, 6H, 2-CH$_3$), 5.64 (d, 1H, J = 10.10 Hz, H-2′), 6.48 (s, 1H, H-4), 6.72 (d, 1H, J = 10.10 Hz, H-1′), 7.47 (dd, 1H, J = 7.90, 7.90 Hz, H-7), 8.31 (dd, 1H, J = 1.70, 7.90 Hz, H-8), 8.52 (dd, 1H, J = 1.70, 7.90 Hz, H-6), 12.68 (s, 1H 1-OH); ^{13}C NMR (125 MHz, methanol-d_4) δ: 29.68, 72.98, 96.15, 98.08, 98.44, 109.99, 114.94, 126.58, 128.04, 122.91, 128.29, 130.90, 131.38, 134.07, 143.29, 170.53, 178.60; IR (ATR) 3428 (OH), 3021 (CH alkane), 2400 (CH aromatic), 1736 (C = O), 1651 (C = C aromatic), 1520 (NO), 1317 (CN), 1217 (CO) cm^{-1}; DI-MS m/z calcd for $C_{18}H_{13}NO_6$ [M]$^+$ 339.10 found 339.00

2.2.1.6. Synthesis of 1-hydroxy-3′,3′-dimethyl-6-nitropyrano[3,2–b] xanthen-6(2H)-one (6).. Oily brown; 40.00 %; [Eluent: Hexane: Ethyl acetate (9:5)]; ^{1}H NMR (500 MHz, methanol-d_4) δ: 1.50 ppm (s, 6H, 2-CH$_3$), 5.64 (d, 1H, J = 10.10 Hz, H-2′), 6.41 (s, 1H, H-4), 6.73 (d, 1H J = 10.10 Hz, H-1′), 8.16 (dd, 1H, J = 2.15, 8.70 Hz, H-7), 8.30 (d, 1H, J = 2.15 Hz, H-5), 8.41 (d, 1H, J = 8.70 Hz, H-8), 12.76 (s, 1H, 1-OH); ^{13}C NMR (125 MHz, methanol-d_4) δ: 29.68, 78.90, 95.52, 103.97, 106.26, 114.99, 113.71, 108.91, 124.60, 118.07, 127.68, 128.14, 155.38, 157.14, 157.70, 161.83, 179.05; IR (ATR) 3435 (OH alcohol), 3021 (CH alkane), 2360 (CH aromatic), 1650 (C = O), 1530 (NO), 1430 (C = C aromatic), 1315 (CN), 1217(CO) cm^{-1}; DI-MS m/z calcd for $C_{18}H_{13}NO_6$ [M]$^+$ 339.10 found 339.00

2.2.2. Structure determination by single-crystal XRD analysis

The 7-nitro-1,3-dihydroxy-9H-xanthen-9-one (**1**) was chosen for confirmation and analysis of the chemical bonding of the structure as it is the most active. The compound **1** crystal is suitable for single crystal analysis that was grown from hexane and ethyl acetate in a slow evaporation method and characterized crystallographically. The diffraction data were measured at T = 301 K on a Bruker APEX-II CCD diffractometer fitted with Mo Kα radiation (λ = 0.71073 Å). Then, data reduction, including analytical absorption correction, was done via multi-scan using SADABS-2016/2 (Bruker,2016/2) [43]. The structures were solved by direct methods and refined (anisotropic displacement parameters, C-bound H atoms in the riding model approximation) on F2 [44]. The oxygen and nitrogen-bound hydrogen atoms were located from Fourier difference maps and refined with distance restraints of O–H = 0.84 ± 0.01 Å and N–H = 0.88 ± 0.01 Å. In the final cycles of the refinement of 10, two reflections, i.e. (−6—4 8), were omitted due to poor agreement with the model.

Table 5
The percentage of dead brine shrimp of compound 1.

Sample Concentration (μM)	Number of dead shrimp/ Total of shrimp								
	3660.35	1830.18	915.09	457.54	228.77	114.39	57.21	28.59	Untreated Control
1	All survive	All survive	All survive	All survive	All survive	All survive	All survive	All survive	All survive
2									
3									
4									
5									
6									
Total									
Percentage of dead shrimp	0 %	0 %	0 %	0 %	0 %	0 %	0 %	0 %	0 %

2.3. Bioassay

2.3.1. Cell culture

The cell lines used in this research were immortalized human keratinocyte (HaCaT), macrophage (RAW 264.7), and the breast cancer cell lines oestrogen-receptor positive (MCF-7) and triple-negative (MDA-MB-23). The cell lines were cultured in RPMI 1640 medium supplemented with 0 % fetal bovine serum and 50 units/mL penicillin–streptomycin mixture (Invitrogen Co., Carlsbad, CA, USA) for growth. The cells were maintained in a humidified 5 % CO_2 incubator at 37 °C. All cell lines were sourced from the Department of Medicine, Faculty of Medicine and Health Sciences, Universiti Putra Malaysia.

2.3.2. Microculture MTT (tetrazolium) assay

The assay protocol was performed according to Razak NA (2019) [45]. Initially, 96-well microplates were prepared with different cell lines, and the cells underwent overnight incubation at 37 °C with 5 % CO_2. Gemcitabine (Food & Drug Administration, FDA approved drug. Application number: 200795Orig1s000) [46] and DMSO were used as a positive and negative control. Synthetic derivatives were initially screened at a concentration of 10 μM. Compounds showing less than 50 % cell viability underwent a full dose–response analysis with concentrations ranging from 0.1 to 100 μM to determine their IC_{50} values. The derivatives were prepared by adding 20 μL of stock solutions (100 mg/mL in DMSO) to each well of the microplate containing 180 μL of RPMI 1640 medium. Control wells contained only 180 μL medium, and each derivative concentration was tested in quadruplet. The plates were then incubated for 96 h at 37 °C with 5 % CO_2. After incubation, 50 μL of MTT solution (2 mg/mL in PBS) was added to each well and incubated for 2–4 h at 37 °C. Excess MTT solution was removed, 100 μL of DMSO was added to each well and gently agitated to dissolve the formazan crystals. The absorbance of formazan was measured at 570 nm using a microplate reader to determine cell viability [47]. Cell viability percentage was determined using the formula:

$$\%Cytotyxicity = \frac{Absorbance\ of\ the\ treated\ cells}{Absorbance\ of\ the\ control\ cells} \times 100$$

2.3.3. Toxicity analysis

2.3.3.1. Cytotoxicity.
The selectivity index (SI) needs to be determined to investigate the toxicity of the synthesized compound. The IC_{50} values of the standard and selected compounds on the cancer cells were utilized to identify the SI value by comparing the IC_{50} value on normal cell lines (HaCaT and RAW 264.7). The SI value was calculated using the equation below [48].

$$Selectivity\ index\ (SI) = \frac{IC_{50}\ of\ normal\ cell\ lines\ (\mu M)}{IC_{50}\ of\ cancer\ cell\ lines\ (\mu M)}$$

2.3.3.2. Brine shrimp lethality assay (BSLA).
The Brine Shrimp Lethality Assay (BSLA) was employed to predict the toxicity potential [49] of the chosen synthesized compound. Artemia salina (brine shrimp) larvae

hatched within 24 h [50]. Each of the 96 wells was infused with a 100 μL brine solution containing five to ten brine shrimps. Subsequently, 100 μL of the sample, dissolved in 5 % DMSO, was introduced into the 96 wells with varied concentrations (3660.35, 1830.18, 915.09, 457.54, 228.77, 114.38, 57.21, and 28.59 μM). After 24 h, the wells were inspected using a microscope, and the surviving brine shrimp count in each well was recorded. The lethality percentage of the brine shrimp at each concentration and control was computed, and the lethality concentration (LC_{50}) was established.

2.3.3.3. Zebrafish embryo toxicity assay.
Zebrafish embryos (Danio rerio) at 24 h post-fertilisation (hpf) were examined using an inverted microscope (Olympus CKX 41) and then carefully selected and transferred into individual wells of 96-well microplates using a Pasteur pipette. Both synthesised compound and control treatments were added to the wells, each with varying concentrations. The development of treated embryos was observed at 24, 48, 72, and 96 h post-fertilisation (hpf) to assess formation and development. Parameters such as the survival rate, hatching rate, oedema formation, scoliosis, and heartbeats per minute were monitored. The experiments were conducted in triplicate, and results were presented as mean ± standard deviation (n = 3). The LC_{50} for both samples and controls were determined using probit analysis with linear regression. Statistical significance was assessed using one-way analysis of variance (ANOVA), with $p < 0.05$ considered significant [51,52].

2.4. Molecular docking analysis

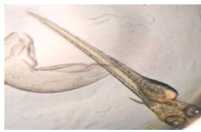#### 2.4.1. Preparation of protein structure
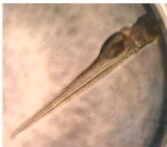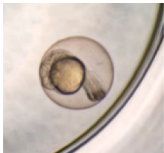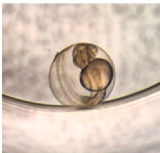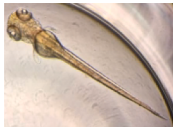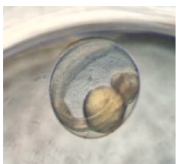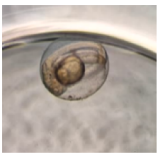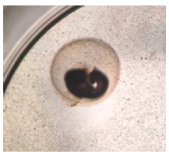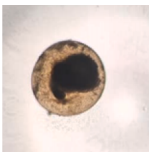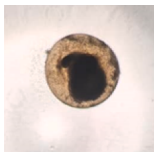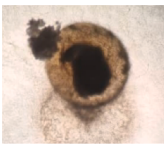
The molecular configuration of the protein was sourced from the RSCB Protein Data Bank under the PDB ID: 3EQM (http://www.rcsb.org/) [53]. The potential binding interactions of the synthesised compounds with the 3EQM protein were explored through molecular docking analysis. This analysis was performed using the AutoDockTools 1.5.4 (https://mgltools.scripps.edu) and AutoDock Vina (https://vina.scripps.edu, respectively) programs. The crystal structure was prepared for molecular docking using BIOVIA Discovery Studio Visualiser. This involved the removal of all water molecules, and the prepared structure was saved in.pdbqt format [54]. Water molecules were removed from the crystal structure to simplify the computational process and to ensure a clear binding site, which could otherwise interfere with the docking search. This step was taken to enhance the accuracy and efficiency of the molecular docking simulations [55]. The final step involved adding hydrogen atoms necessary for forming hydrogen bonds to ensure that the molecular structures are complete and accurate for the docking simulations, enhancing the reliability of the results using AutoDockTools 1.5.4 software [56].

2.4.2. Preparation of ligand structure

The 3D structures of the synthesised compounds were created using the Avogadro program [57]. An energy optimisation tool within the program was then employed to stabilise the ligands' 3D structures,

Table 6

The morphological characteristics of zebrafish embryos treated with six concentrations of compound 1 at 24, 48, 72 and 96 h observed under 5x magnification.

No	Concentration (μM)	Duration			
		24 Hrs	48 Hrs	72 Hrs	96 Hrs
1	EM with 0.1 % DMSO (Control)				
2	28.59				
3	57.21				
4	114.39				
5	228.77				
6	457.54				
7	915.09				
8	1830.18				

preparing them for molecular docking studies [58]. Subsequently, all ligands were transformed into.pdbqt file format for molecular docking.

2.4.3. Molecular docking of ligand and protein

In a molecular docking study, AutoDock Vina was used to dock optimised ligand molecules that were docked into a refined protein model. This process aimed to identify the best ligand conformations within the binding sites of the target macromolecules (3EQM) and determine the affinity energy of the interactions. In order to identify the binding pocket of the target receptor, the protein structure was initially loaded, and then the active site was located based on the location of the co-crystallised ligand [59]. The grid box of the receptor (3EQM) is shown as follows: RMSD: 1 Å, the size of the grid box: x-axis: 40.00, y-axis: 40.00 and z-axis: 40.00 and the centre-x: 85.51, centre-y: 51.58 and centre-z: 43.04. The analogues were then subjected to Biovia Discovery Studio Visualiser to view lists of interactions and better ligand–protein

Compound	Binding Affinity (kcal/mol)
1	−8.4
2	−7.8
3	−8.1
4	−8.4
5	−8.1
6	−8.2
Letrozole	−8.3

residue graphics in both 2D and 3D representations. AutoDock Vina was used to re-dock the isolated co-crystallized ligands into the corresponding protein binding sites after they were prepared following the same standard protocol for ligand preparation. For the purpose of validating the docking procedure, the docked pose was superimposed over the original pose to calculate the Root Mean Square Deviation (RMSD) for the protein 3EQM.

3. Results and discussion

3.1. The synthesis and characterization of nitro xanthone derivatives

A total of six xanthone derivatives were synthesized and characterized (**1–6**), but we only focused on the most potent and non-toxic compound in this article which is compound **1**. The spectral values of compounds **2–6** are given in the experimental synthesis section and supplementary data (**Figs. S5-S24**). Briefly, the process of generating compound **1** involved the one-pot reaction combining 5-nitrosalicylic acid and phloroglucinol followed by the addition of a coupling agent and catalyst, i.e., Eaton's reagent [38–40] comprising phosphorus pentoxide solution in methane sulfonic acid (P$_2$O$_5$/CH$_3$SOH) (Scheme 1). The cyclization reaction was involved in the synthesis of xanthone derivatives. At the end of this reaction, tricyclic xanthone **1** was produced with a yield of 78 %.

After synthesis, nuclear magnetic resonance spectroscopy (^{1}H and ^{13}C NMR), Fourier transform infrared spectroscopy (FTIR), and direct infusion-tandem mass spectrometry (DI-MS) studies were used to characterize and elucidate the purified compounds. Compound **1** exhibits five signals spanning from 6.00 to 9.00 ppm, representing five aromatic protons, as shown in ^{1}H NMR (**Fig. S1**; Supporting document). The signals are observed at 8.80 ppm (1H, d, *J* = 2.75 Hz), 8.60 ppm (1H, dd, *J* = 2.75, 9.25 Hz), 7.83 ppm (1H, d, *J* = 9.25), 6.48 ppm (1H, d, *J* = 1.95 Hz), and 6.29 ppm (1H, d, *J* = 1.95 Hz), assigned respectively as H-8, H-6, H-5, H-2, and H-4. A broad signal at 12.40 (2H, s) corresponds to the two hydroxyl protons of 1-OH and 3-OH.

The ^{13}C NMR analysis (**Fig. S2**; Supporting document) revealed distinct peaks corresponding to different carbon environments in the compound. The carbonyl carbon C9 exhibits the highest chemical shift at 178.78 ppm. Hydroxyl carbons C1 and C3 appeared at 166.75 and 159.00 ppm due to the deshielding effects of the hydroxyl groups. Carbon C7, associated with the nitro (NO$_2$) group, is observed at 129.46 ppm. Meanwhile, carbons C5, C6, and C8, located on the same aromatic ring, appeared at 121.42, 126.39, and 128.92 ppm, with C6 and C8 showing slightly higher chemical shifts due to their proximity to the –NO$_2$ group. Quaternary carbons C10a, C4a, C8a, and C9a are observed at the peaks of 139.60, 109.99, 98.64, and 94.40 ppm, with C10a and C4a exhibiting higher chemical shifts due to their oxygen bonding. Carbons C2 and C4, located on the same aromatic ring, appeared at 119.12 and 117.73 ppm, where C2 is slightly deshielded, likely due to its position between two hydroxyl-bonded carbons.

The FTIR analysis (**Fig. S3**; Supporting document) shows O-H stretching at 3337 cm-1, C-H stretching at 2359 cm^{-1}, C = O stretching at 1620 cm^{-1}, C = C stretching at 1528 cm^{-1}, N-O stretching at 1446 cm^{-1}, C-N stretching at 1265 cm^{-1}, and C-O stretching at 1216 cm^{-1}, indicating the presence of various functional groups in the compound. The DI-MS spectrum (**Fig. S4**; Supporting document) displays a molecular ion peak [M]$^+$ and a base peak at *m/z* 273.00, congruent to the expected molecular formula of C$_{13}$H$_7$NO$_6$ for the compound [42].

3.2. X-ray diffraction (XRD) analysis

High quality crystal form of compound **1** was grown via the slow evaporation method, where it was dissolved in ethyl acetate and kept at room temperature to allow slow evaporation of the solvent. The solution and refinement of the single crystal data of compound **1** confirmed the molecular structure of the compound to be agreeable to other data obtained earlier. Refinement of the crystal structure led to a final R factor of 5.14 %. The molecular structure of compound **1** is depicted in ORTEP view (Fig. 2). The compound is found to crystallize in a monoclinic system with a C2/c space group. The asymmetric unit constitutes one molecule of **1** in a neutral state. The complete unit cell contains eight molecules, as shown in Fig. 2. The analysis of single-crystal X-ray diffraction revealed that **1** has three cyclic rings with aromaticity on the side ring. Each element within the ring has a p-orbital that is perpendicular to the ring; hence, **1** is planar, as depicted in Fig. 3. Metrical parameter analysis indicates that the molecule does not display any anomalies compared to the available literature data for related compounds. Table 2 lists the details of the crystal data collection and structure refinement.
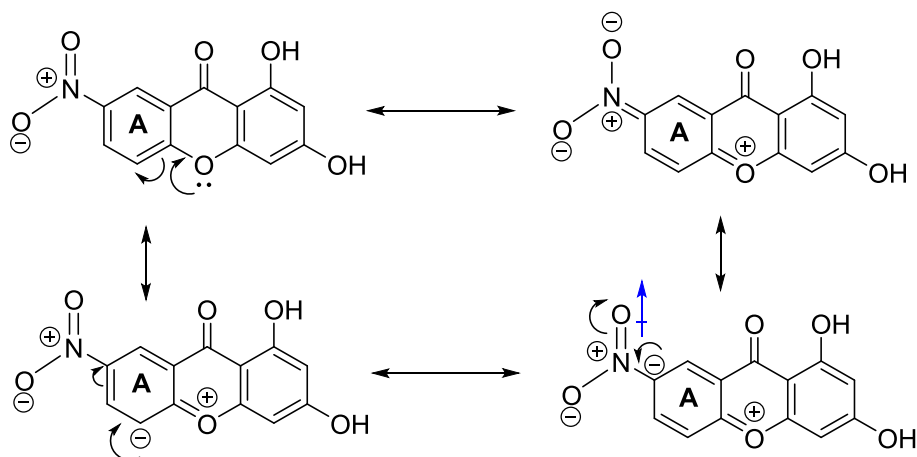
Fig. 4. Electron density effect of *para*-nitroxanthone (1).
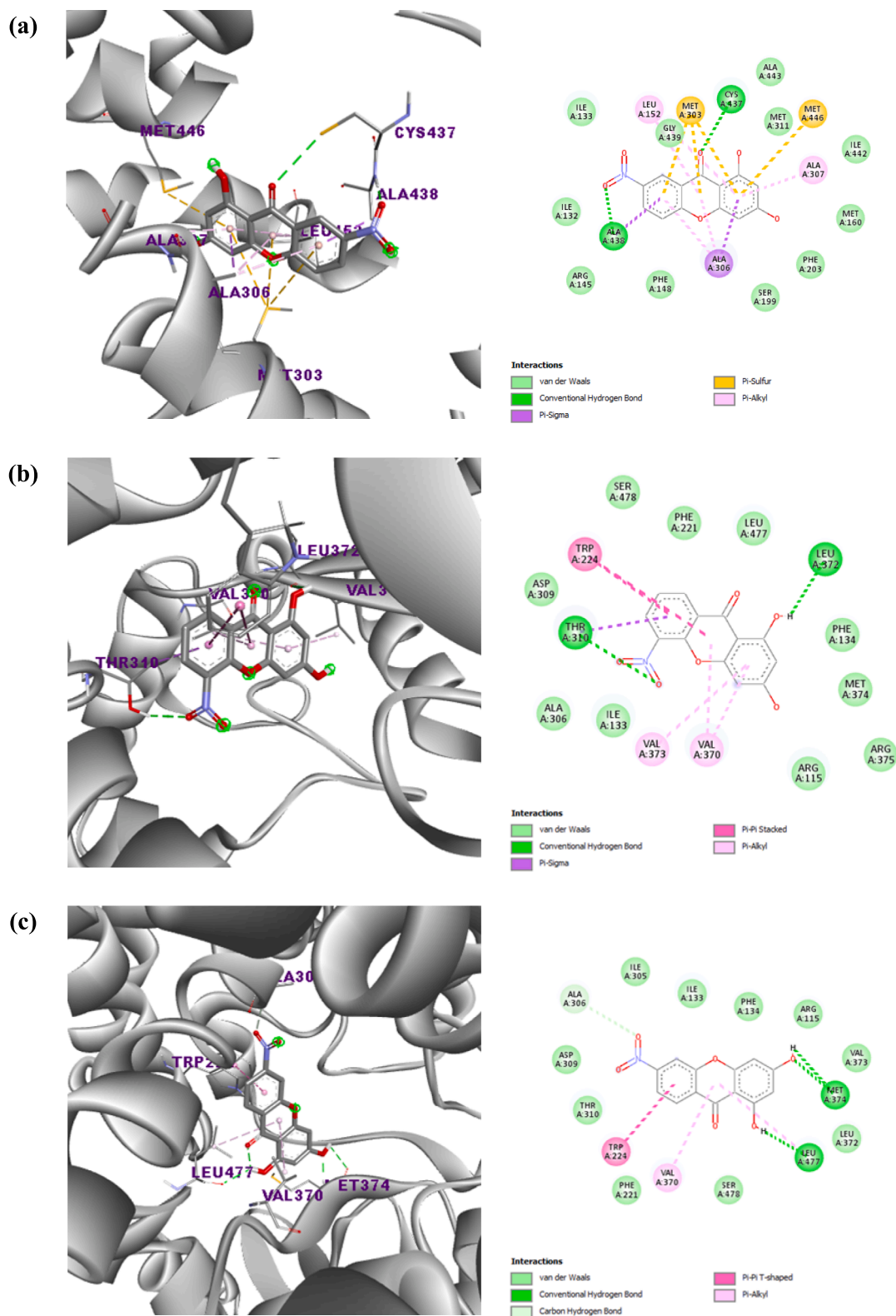
Fig. 5. Active site analysis and drug interactions of human placental aromatase cytochrome P450 (PDB ID: 3EQM). (a) Docked conformation of compound 1 together with the key amino acid residues of human placental aromatase cytochrome P450. (b) Docked conformation of compound 2 together with the key amino acid residues of human placental aromatase cytochrome P450. (c) Docked conformation of compound 3 together with the key amino acid residues of human placental aromatase cytochrome P450. (d) Docked conformation of compound 4 together with the key amino acid residues of human placental aromatase cytochrome P450. (e) Docked conformation of compound 5 together with the key amino acid residues of human placental aromatase cytochrome P450. (f) Docked conformation of compound 6 together with the key amino acid residues of human placental aromatase cytochrome P450. (g) Docked conformation of letrozole together with the key amino acid residues of human placental aromatase cytochrome P450. (h) Comparison of binding location between compounds 1–6 and the potential aromatase inhibitor, letrozole.

(d)

(e)

(f)
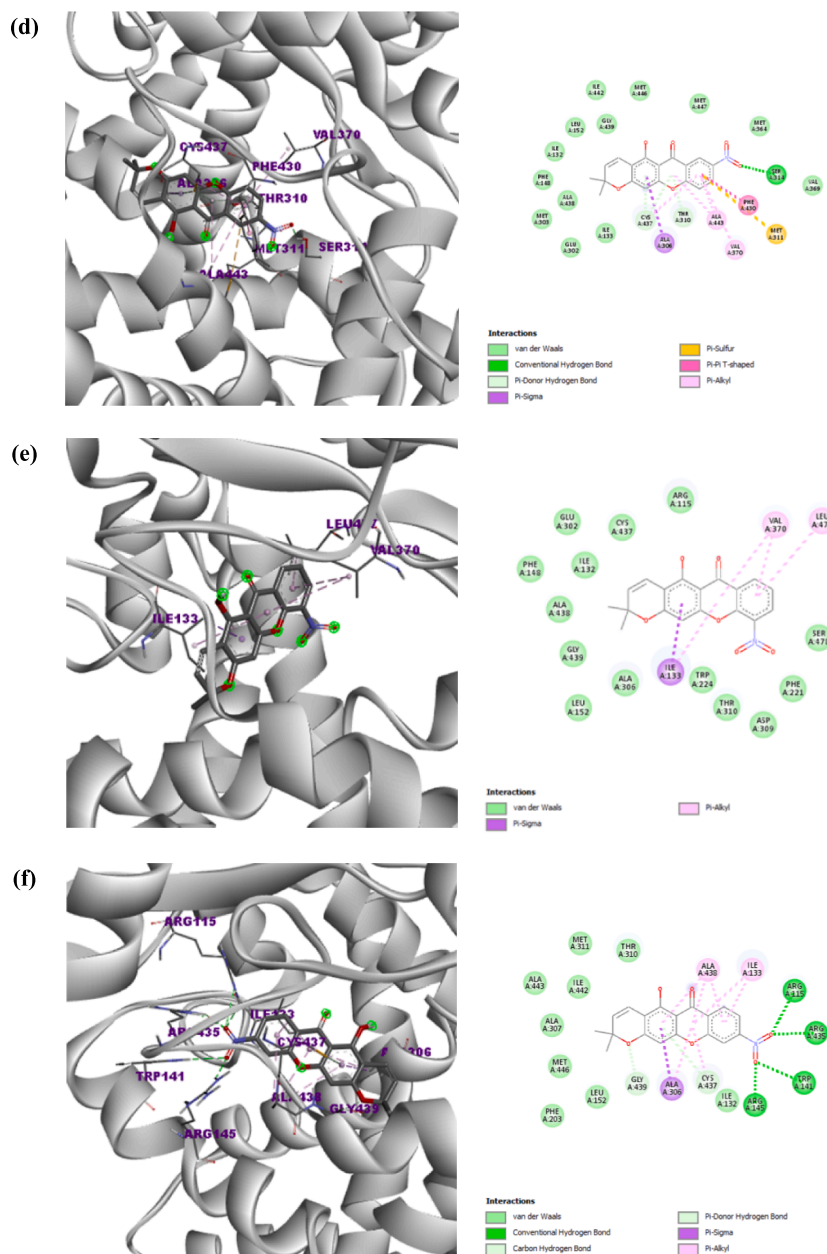
Fig. 5. (*continued*).

3.3. Preliminary screening of the synthetic derivatives (1–6) against breast cancer cell lines (MCF-7 and MDA-MB-231)

The compounds were studied for their potencies in inhibiting breast cancer cell lines by screening assay at 10 μM concentration. The breast cancer cell lines used in this study were MCF-7 (estrogen receptor-positive) and MDA-MB-231 (triple-negative). The *in vitro* cytotoxicity of compounds **1–6** was tested using the MTT 3-(4,5-dimethylthiazol-2-yl)-2,5-diphenyltetrazolium bromide assay. A chemotherapy drug, gemcitabine, was used in this study as a positive control. Table 3 shows the percentage of cell viability of compounds **1–6** against two different cell lines, MCF-7 and MDA-MB-231, at a concentration of 10 μM.

According to Riss T.L (2013) [60], a compound is regarded as an active compound if the viability of the cells after the screening test is less than 50 %. Compound **1** exhibits the greatest inhibitory effect against MCF-7 compared to the other compounds (**2–6**) in the screening test (Table 3), as it was applied at 10 μM to MCF-7 cells, resulting in a viability rate of 22.05 % ± 2.40 %. This rate is influenced by cellular

activity in the cytoplasm, particularly where estradiol, a type of estrogen, undergoes metabolic or functional processes. Compound **1**′s presence or activity in this cellular context impacts MCF-7 cell viability, potentially through interactions with estradiol metabolism or cytoplasmic signaling pathways. Interestingly, compound **1** shows a similar percentage of cell viability as gemcitabine, a standard drug, in Table 3. In contrast, compound **1** has no inhibitory effects against MDA-MB-231, with a cell viability percentage of 98.92 ± 2.00 %. The MDA-MB-231 is a cell line that is resistant to treatment with antiestrogens because it lacks an estrogen receptor (ER). It is also a triple-negative breast cancer cell line, i.e., none of the usual breast cancer receptors are present.

Based on the SAR analysis, this also verifies that the insertion of the nitro group at the *para* position (compound **1**) of the precursor compound increased its activity. In contrast, compounds **2** to **6** showed no activity against MCF-7 cells, as shown in Table 3. Although the nitro group as the electron-withdrawing group was presented in both compounds (**2 and 3**), the greater steric hindrance at the *ortho* and *meta* positions (nitro group and ring B) likely retards the interaction of the

(g)

h)
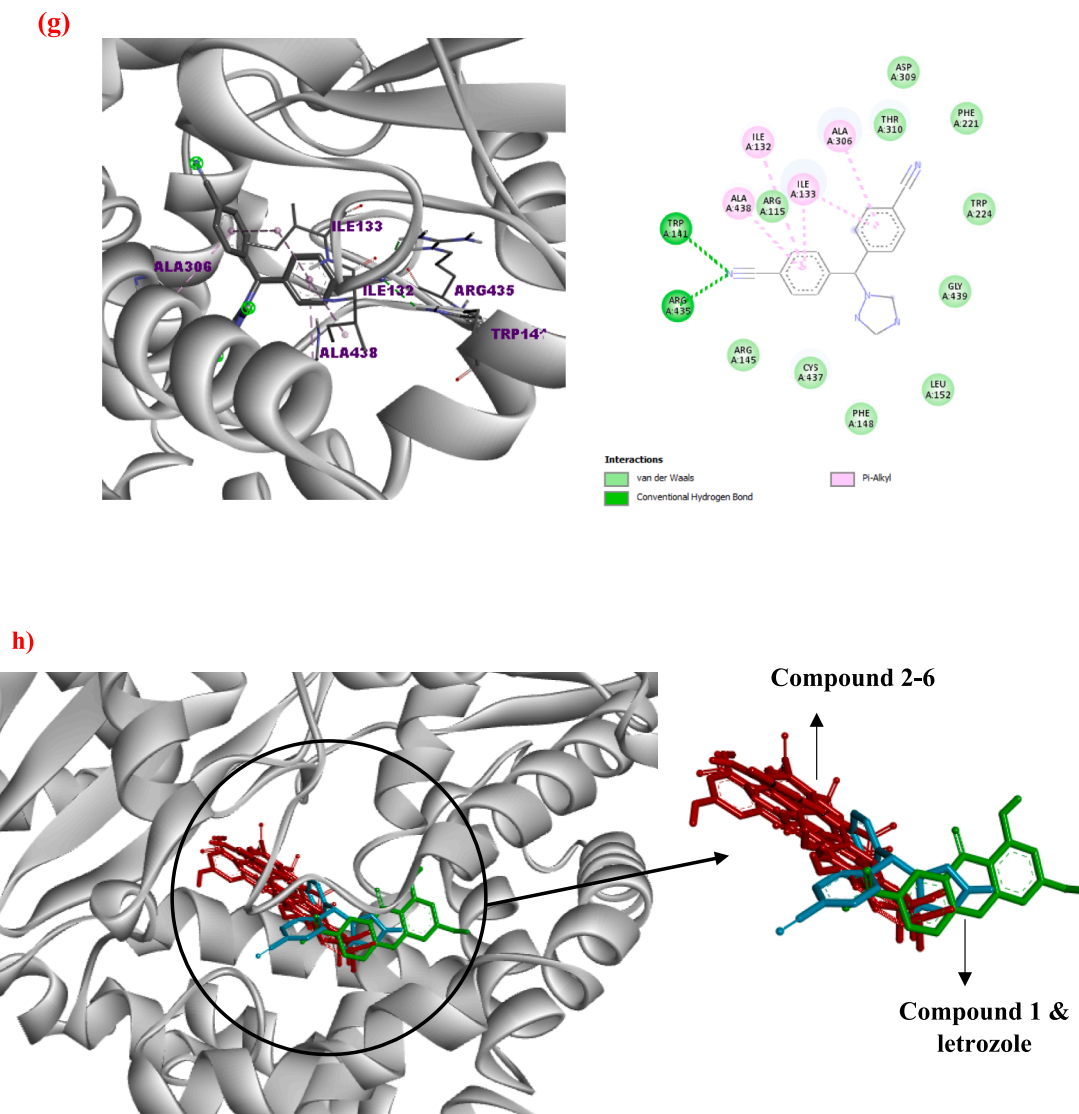
Fig. 5. (*continued*).

aromatic ring A with MCF-7 cells [61]. Another possible theory is the electron density effect, in which any conjugate of the lone pair on the O atom with the π system would increase the electron density in the *ortho* and *para* positions, but mostly favored *para* which is more reactive (Fig. 5) [62]. Interestingly, compound **4** has the same position of the nitro groups as compound **1**, but unfortunately, it does not show activity against MCF-7. We suspect that adding an alkylation group (EDG) on the D ring may cause low electron density on the oxygen atom because the lower the stabilization energy, the less reactive compound **4** [63].

To evaluate the safety of the active compound, the cytotoxicity of compound **1** and gemcitabine was assessed on the normal lung cell line BEAS-2B (Table 4). Compound **1** showed a higher percentage of cell viability, 94.15 %, compared to gemcitabine, which had 9.64 %. Based on Riss T.L. (2013) [60], this means that compound **1** is not toxic to normal cells, while gemcitabine is highly toxic to normal cells. This is very interesting because compound **1** shows potential for novel applications compared to the standard drug (gemcitabine), specifically being selectively toxic to the MCF-7 breast cancer cell line only.

3.4. Half-maximal inhibitory concentration IC_{50} value

The selection of the synthetic compound **1**, which showed inhibitory efficacy against the oestrogen-dependent breast cancer (MCF-7) cell line (Table 3), was subsequently examined at various concentrations (0.1, 1, 10, and 100 μM) to identify its half-maximal inhibitory concentration value, IC_{50}. **Fig. S25** presents that the IC_{50} value of compound **1** that inhibits the growth of oestrogen-dependent breast cancer cells (MCF-7) is 7.00 ± 0.00 μM. Meanwhile, based on study by Tao et al group, the $IC_{50}'s$ of gemcitabine against MCF-7 was 2.01 ± 0.30 μM [64].

Previous research has indicated that an IC_{50} value of less than 10 μM is deemed highly inhibitory against cancer cells [65]. Thus, compound **1** demonstrated good cytotoxicity with a promising percentage of cell death towards MCF-7 [66]. However, the effects of the synthetic compound **1** on normal cell lines need to be determined via *in vitro* cytotoxicity assay.

3.5. Cytotoxicity and selectivity index (SI) on normal cell lines

The selectivity index of compound **1** against normal cell lines was conducted using the MTT assay. The cell lines used were human epidermal keratinocyte (HaCaT) and macrophage (RAW 264.7) from the American Tissue Culture Collection (Virginia, USA). **Fig. S26** and **Fig. S27** present the IC_{50} value of compound **1** against HaCaT and RAW 264.7 (normal cell lines) as 250.00 ± 70.71 and 800.00 ± 0.00 μM, with SI values of 35.71 and 114.29. A compound is considered a good potential inhibitor for the therapeutic agent if its SI value is more than 10

Table 8

The interactions available on molecular docking analysis of letrozole and compound **1–6** with aromatase-androstenedione complex structure (3EQM).

Compounds	Binding Affinity (kcal/mol)	Receptor	Type of interactions	Distance (Å)
1	−8.4	ALA438	H-B	1.89
		CYS437	H-B	3.49
		ALA306	π-Sigma	3.94
		ALA438	π −Sigma	3.88
		LEU152	π −Alkyl	4.87; 5.22
		ALA307	π −Alkyl	4.28
		ALA306	π −Alkyl	3.42; 4.40
		MET303	π −Sulfur	4.87; 5.11; 5.64
		MET446	π −Sulfur	5.40
2	−7.8	THR310	H-B	2.60
		LEU372	H-B	2.70
		THR310	Pi-Sigma	3.95
		TRP224	π − π Stacked	4.80; 5.97
		VAL373	π −Alkyl	5.25
		VAL370	π −Alkyl	4.76; 4.92
3	−8.1	LEU477	H-B	2.14
		MET374	H-B	H: 2.87; O: 1.86
		ALA306	C-H Bond	3.48
		TRP224	π − π T-shaped	4.72
		VAL370	π −Alkyl	5.42
		LEU477	π −Alkyl	5.45
4	−8.4	SER314	H-B	1.93
		THR310	π −Donor H-B	2.66
		CYS437	π −Donor H-B	3.66; 4.02
		ALA306	π −Sigma	3.87
		MET311	π −Sulfur	5.95
		PHE430	π − π T-shaped	5.50
		VAL370	π −Alkyl	5.28
		CYS437	π −Alkyl	5.15
		ALA443	π −Alkyl	5.26; 5.30
5	−8.1	ILE133	π −Sigma	3.67
		VAL370	π −Alkyl	4.62; 5.50
		LEU477	π −Alkyl	5.17
		ILE133	π −Alkyl	4.97
6	−8.2	ARG115	H-B	2.95; 2.38
		TRP141	H-B	2.63
		ARG145	H-B	2.11
		ARG435	H-B	2.05; 2.46
		GLY439	C-H Bond	3.62
		CYS437	π −Donor H-B	4.13
		ALA306	π −Sigma	3.85
		ILE133	π −Alkyl	4.27; 5.12
		ALA438	π −Alkyl	5.14
		ALA306	π −Alkyl	5.25
		CYS437	π −Alkyl	4.76
		ALA438	π −Alkyl	4.75; 5.40
Letrozole	−8.3	TRP141	H-B	2.38
		ARG435	H-B	2.16; 2.77
		ALA306	π −Alkyl	4.67
		ALA438	π −Alkyl	4.59
		ILE132	π −Alkyl	5.37
		ILE133	π −Alkyl	4.49; 4.81

*H-B = Hydrogen bonding; C-H = Carbon-hydrogen.

[48]. From the results, compound **1** has an SI value higher than 10 for HaCaT and RAW 264.7 cell lines. It indicates the uniqueness of compound **1**, i.e., it is more selective to oestrogen-dependent breast cancer cell lines (MCF-7) and nontoxic toward normal cell lines, which is desirable for drug candidates.

3.6. Brine shrimp lethality assay (BSLA)

A brine shrimp lethality assay (BSLA) was performed on compound **1**. It is a simple, high-throughput toxicity assay for bioactive substances [67]. Table 5 displays a 0 % of dead shrimps for various concentrations of compound **1**. The mortality rate was recorded based on this preliminary data. Crude or pure compounds are considered toxic if their

Table 9

The ADMET properties of compound 1.

ADMET properties	Value	Outcome
Absorption		
Plasma Protein Binding	95.50 %	High therapeutic index
Blood-Brain Barrier	0.670	BBB-
Human Intestinal Absorption	0.009	HIA-
Caco-2 Permeability	−4.860	Caco2-
P-Glycoprotein Inhibitor	0.002	Non-inhibitor
P-Glycoprotein Substrate	0.080	Non-substrate
Metabolism		
CYPA2 inhibitor	0.980	Inhibitor
CYPA2 substrate	0.680	Substrate
CYP2C9 inhibitor	0.404	Non-inhibitor
CYP2C9 substrate	0.058	Non-substrate
CYP2C9 inhibitor	0.600	Inhibitor
CYP2C9 substrate	0.930	Substrate
CYP2D6 inhibitor	0.739	Non-inhibitor
CYP2D6 substrate	0.453	Non-substrate
CYP3A4 inhibitor	0.647	Non-inhibitor
CYP3A4 substrate	0.090	Non-substrate
Toxicity		
AMES Toxicity	0.879	Non-Toxic
Human Ether-à-go-go-Related Gene Inhibition (hREG I//II inhibitor)	0.060	Inactive (Weak inhibitor)
Eye Corrosion	0.283	Noncorrosive

Table 10

The drug-likeness analysis of compound 1.

Druglikeness	Results
Lipinski	Yes; 0 violation
Ghose	Yes
Veber	Yes
Egan	Yes
Muegge	Yes
Bioavailability Score	0.55

lethal concentration (LC$_{50}$) value is < 3660.35 μM and non-toxic if their LC$_{50}$ value is > 3660.35 μM [68]. Our finding revealed that compound **1** had no toxicity against brine shrimp. The finding signifies that compound **1** is inactive towards the brine shrimp even at the highest concentration used (3660.35 μM), and there is no observed fatality of the brine shrimps. For increased accuracy and avoidance of different data produced, the lethality assay was performed in six replicates to avoid inconsistency in the results received.

3.7. Zebrafish embryo toxicity test

Compound **1** was tested at various concentrations to assess its effect on zebrafish embryo survival rate over 96 h. The results showed a 100 % survival rate at concentrations between 57.21 to 228.77 μM, similar to the negative control (embryos treated with 0.1 % DMSO). However, survival decreased to 50 % at 915.09 μM, and no embryos survived at the highest concentration of 1830.18 μM. This pattern of survival was consistent across the tested concentrations, highlighting the resilience of most embryos to compound **1**. The LC$_{50}$ value of compound **1** for zebrafish embryos was determined to be 474.43 μg/mL over 96 h. ANOVA analysis confirmed this value, indicating that compound **1** is non-toxic to zebrafish embryos, even after prolonged exposure up to 96 h post-fertilization, as shown in Fig. S28.

Figs. S28 and S29 present the effects of compound **1** on zebrafish embryos. In Fig. S30, hatching rates were 25 % at concentrations between 28.59 and 228.77 μM after 48 h, improving to 100 % between 72 and 96 h. At 457.54 μM, the hatching rate decreased to 66.67 %, and at 915.09 μM, it was 50 %. No embryos hatched at 1830.18 μM. Fig. S31 shows heartbeat measurements at the 96-hour mark, revealing no significant changes in surviving embryos at concentrations from 28.59 to
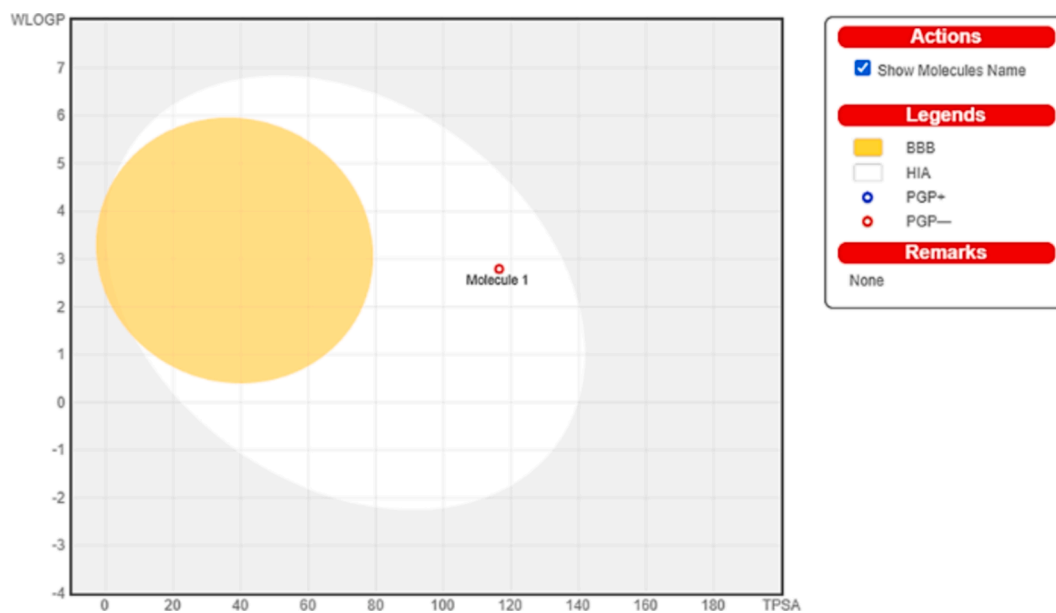
Fig. 6. The boiled egg model of compound 1.

915.05 μM. At 1830.18 μM, no heartbeat was detected in deceased embryos. The data indicate a decrease in heartbeat as the concentration increased, with the LC_{50} value of compound **1** (474.43 μg/mL or 1736.58 μM) falling within the non-toxic range of 915.05 to 1830.18 μM [69].

The morphological features of zebrafish embryos exposed to various concentrations of compound **1** (0 to 1830.18 μM) were assessed over 24 to 96 h. No morphological changes, such as scoliosis, pericardial oedema, or coagulation, were observed, indicating that the embryos survived well up to 96 h. At the pharyngula stage, fin growth and the development of blood circulation organs were seen even at the highest concentration of compound **1**. By 72 to 96 h, the hatched embryos displayed active feeding behaviour and growth across all concentrations. However, at 1830.18 μM, no embryos hatched during the 24 to 96-hour period. A summary of the findings is provided in Table 6.

3.8. Molecular docking

To visualize the detailed intermolecular interactions between the synthesized compounds (**1**–**6**), the molecular docking analysis was performed using the crystal structure of human placental aromatase cytochrome P450 (PDB ID: 3EQM; 2.90 Å X-ray resolution) using the Autodock Vina software [70]. Firstly, the RMSD value calculated for co-crystallized ligand pose vs docked posed was 2.892 Å. According to Ramírez & Caballero (2018), the RMSD value < 2.0 Å agrees with good docking solutions and the docking solutions with an RMSD value between 2.0 to 3.0 Å maintain the intended orientation while varying from the reference position [71]. Therefore, acceptable RMSD values were found for the chosen docking protocol, demonstrating its capacity to replicate the initial co-crystallized position.

Based on the binding affinity values from Table 7, it is evidenced that compound **1** where the nitro group at the *para* position showed the highest binding affinity value compared to other compounds where the nitro position at the alternate position. As illustrated in Fig. 4.**a–f**, all the compounds (except compound **5**) have at least one hydrogen bonding interaction with the active site of the protein. However, only compound **1** makes hydrogen bonding with the nitrogen atom of CYS437 through the oxygen atom present at C-9 establishing a bond length of 3.49 Å. This interaction significantly contributed to the overall binding affinity of the compound [72].

Notable, there is a hydrogen bond interaction between the nitro group at the *para* position of compound **1** and ALA438 amino acid residue measured at a bond distance of 1.89 Å. Nevertheless, compound **4** where the position of nitro groups was the same as compound **1** exhibited the same binding affinity as compound **1**, but compound **4** only has one hydrogen bond interaction with a slightly longer bond distance (1.93 Å) compared to compound **1**. Additionally, the nitro group at *ortho* position of compound **2** established two hydrogen bonding interactions with THR310 and LEU372 amino acid residues but the bond distance is relatively longer (bond distance = 2.60 Å; 2.70 Å respectively) than the bond distance of compound **1**. Thus, this factor is evidence that compound **1** with the nitro group at the *para* position was interacting with the active site more efficiently compared to the other compounds. Additionally, the aromatic ring of compound **1** plays a part in a π-sulfur interaction with MET303 and MET446 amino acid residue, apparent from the 4.88 Å, 5.11 Å, 5.64 Å and 5.40 Å bond lengths respectively. On the other hand, as shown in Fig. 4**g**, letrozole, the potential aromatase inhibitor, exhibited two hydrogen bonding interaction with TRP141 and ARG435 amino acid residue. However, both the hydrogen bond interaction has longer bond length (2.38 and 2.16; 2.77 respectively). Due to this weaker interaction, letrozole displayed a slightly lower binding affinity than compound **1**. Table 8 illustrates the key interaction of aromatase inhibitor, letrozole and compounds **1**–**6** with the amino acid residues of the active site.

Moreover, as illustrated in Fig. 4**h**, it is clearly showed that compound **1** (green color) and the aromatase inhibitor, letrozole (blue color) bonded at the same location of the active site compared to the other compounds (red color) which exhibited that compound **1** able to replicate the efficiency in inhibiting the cytochrome P450 same as the potential inhibitor. Thus, these complex interactions within the molecular framework of compound **1** proved that the nitro group at the *para* position exhibited strong binding potential in comparison with compounds **2**–**6**. In order to confirm the docking results on human placental aromatase cytochrome P450, the biochemical validation of aromatase activity for compound **1** must be explored further.

3.9. ADMET properties analysis

The ADMET (absorption, distribution, metabolism, excretion, and toxicity) analysis was applied to identify the predicted toxicity of compound **1** [73]. The ADMET analysis predicted the pharmacokinetic properties and toxicities of the selected compound, including their

permeability for the blood–brain barrier (BBB), human intestinal absorption (HIA), and whether they act as P-glycoprotein substrates or inhibitors. According to the results in Table 9, compound **1** showed negative (−) BBB and HIA permeability, suggesting weak absorption in the human body [74]. Moreover, compound **1**, the most promising molecule identified through docking and bioassay, was found to be a non-inhibitor of P-glycoprotein. It suggests that the molecule is unlikely to interact with other medications or drugs, as P-glycoprotein is often implicated in drug-drug interactions [75]. Furthermore, the ADMET analysis indicates that compound **1** inhibits CYP enzymes, specifically isoforms A2 and 2C9. Inhibition of these enzymes can lead to either enhanced or reduced drug metabolism because human cytochrome P450 (CYP) isoforms A2, 2C9, 2D6, and 3A4 collectively account for approximately 90 % of oxidative metabolic activities [76]. The ADMET results revealed that although the compound showed a high AMES toxic value, it is non-corrosive to the human eye. Finally, the ADMET data indicate that compound **1** is a weak inhibitor and inactive against the Human Ether-à-go-go-Related Gene (hERG). The hERG gene is known to be sensitive to drug interactions [77]. Thus, compound **1** is predicted to have good binding with the receptor [78].

3.10. Drug-likeness analysis

The study further employed pharmacokinetic and drug-likeness predictions according to the Lipinski, Ghose, Veber rules, and bioavailability scores, as illustrated in Table 10. According to the drug-likeness analysis, compound **1** does not violate any of the mentioned rules. Specifically, compound **1** met Lipinski's rule of five, which states that a compound should possess a molecular weight (MW) of less than or equal to 500, a LogP value (octanol–water partition coefficient) of less than or equal to 5, fewer than 10 hydrogen bond acceptors, and fewer than 5 hydrogen bond donors [79]. Next, compound **1** agrees with Veber's rules because it has a total hydrogen bond of ≤ 12, rotatable bonds of ≤ 10, and a polar surface area (PSA) of < 140, with oral bioavailability of > 20 % [80]. Moreover, compound **1** falls within the acceptable ranges for Log P (−0.4–5.6), molar refractivity (MR) of 40–150, molecular weight (MW) of 160–480, and number of atoms (20–70), aligning with Ghose's rule [81].

3.11. Gastrointestinal absorption and brain penetration prediction [BOILED-Egg]

The Brain or IntestinaL EstimateD permeation method (BOILED-Egg) method, utilized to assess the pharmacokinetic features, facilitates the comprehension of how the molecule positions in the WLOGP-versus-TPSA referential and small molecule lipophilicity and polarity calculations affect BBB and passive HIA [82]. Moreover, the BOILED-Egg model offers a fast, reliable, and statistically improved method for assessing the high gastrointestinal absorption and brain permeability of small compounds used in drug discovery and development. The yolk (yellow) region indicates a high potential for brain penetration, while the white region indicates a high possibility of passive absorption by the gastrointestinal system. There is no conflict between the white and yolk regions. Fig. 6. depicts compound **1** in the white region, indicating that it is predicted to be highly absorbed by the gastrointestinal tract. P-glycoprotein is important for both the absorption and disposal of drugs. Due to its location, P-glycoprotein apparently could greatly limit the number of drugs absorbed by cells from the intestinal lumen and brain than enhancing drug excretion drugs hepatocytes and renal tubules into the surrounding luminal space. The BOILED-Egg model suggests that compound **1** is not a P-glycoprotein substrate; hence, drug excretion will not be a concern [83].

4. Conclusion

In conclusion, the findings of this study indicate that the nitroxanthone derivatives **1** where the nitro group substituted at *para* position showed similar evidence of a notable anti-breast cancer effect against MCF-7 when compared to the standard drug, gemcitabine, in the screening test in terms of cell viability percentage. Further insights into the half-maximal inhibitory concentration value, IC_{50}, of compound **1** for anti-breast cancer activity was less than 10 µM, confirming compound **1** as having the potential to inhibit breast cancer cell growth. Prior to that, the toxicity analyses of compound **1** on three different models (cell cytotoxicity, brine shrimp, and zebrafish toxicity) were established, revealing compound **1** to be more selective towards breast cancer cell lines than normal cell lines compared to the standard drug (gemcitabine). Compound **1** is corroborated to be non-toxic towards normal cells compared to gemcitabine. Additionally, no mortality was observed in brine shrimp exposed to various concentrations of compound **1**, indicating its inactivity even at the highest concentration tested. Furthermore, the *in vivo* zebrafish embryo toxicity analysis confirmed that compound **1** is non-toxic as per the following parameters: survival rate, hatching rate, heartbeat rate, and morphology. Molecular docking was conducted to elucidate the desired xanthone derivative's binding affinity and chemical interactions. The outcome showed that the docking of compound **1** with nitro group at the *para* position with the crystal structure of human placental aromatase cytochrome P450 (PDB ID: 3EQM), showed a significantly better binding affinity than compound **2–6** with nitro group at the alternate position. Lastly, the potential of compound **1** as a drug candidate was also evaluated by calculating and verifying their adherence to Lipinski's rule. Thus, integrating pharmacokinetic and molecular docking analysis verifies *in vitro* findings and enhances the potential of these compounds in medicinal applications. This multifaceted strategy lays the groundwork for future research and therapeutic applications.

CRediT authorship contribution statement

Pavithren Devakrishnan: Writing – original draft, Methodology, Investigation. **Nadiah Mad Nasir:** Writing – review & editing, Supervision, Project administration, Funding acquisition, Conceptualization. **Johnson Stanslas:** Validation, Methodology, Data curation. **Muhammad Alif M. Latif:** Validation, Methodology, Data curation. **Ahmad Zaidi Ismail:** Validation, Data curation. **Fatin Farhana Baharuddin:** Writing – review & editing, Methodology.

Declaration of competing interest

The authors declare the following financial interests/personal relationships which may be considered as potential competing interests: Nadiah Mad Nasir reports financial support was provided by Ministry of Higher Education Malaysia, Fundamental Research Grant Scheme (FRGS). If there are other authors, they declare that they have no known competing financial interests or personal relationships that could have appeared to influence the work reported in this paper.

Appendix A. Supplementary data

Supplementary data to this article can be found online at https://doi.org/10.1016/j.rechem.2024.101998.

Data availability

I have attached the supporting document

References

[1] A. Howell, A.S. Anderson, R.B. Clarke, S.W. Duffy, D.G. Evans, M. Garcia-Closas, et al., Risk determination and prevention of breast cancer, Breast Cancer Res. 16 (5) (2014 Oct 28) 446.

[2] H. Sung, J. Ferlay, R.L. Siegel, M. Laversanne, I. Soerjomataram, A. Jemal, et al., Global Cancer Statistics 2020: GLOBOCAN Estimates of Incidence and Mortality Worldwide for 36 Cancers in 185 Countries, CA Cancer J Clin. 71 (3) (2021 May 4) 209–249.

[3] World Health Organization [internet]. (2024).

[4] R.L. Siegel, K.D. Miller, A. Jemal, Cancer statistics, 2019, CA Cancer J Clin. 69 (1) (2019 Jan 8) 7–34.

[5] J. Geisler, Differences between the non-steroidal aromatase inhibitors anastrozole and letrozole – of clinical importance? Br J Cancer. 104 (7) (2011 Mar 1) 1059–1066.

[6] A.C. Lissaman, J.E. Girling, L.M. Cree, R.E. Campbell, A.P. Ponnampalam, Androgen signalling in the ovaries and endometrium, Mol Hum Reprod. (2023). May 31;29(6.

[7] I. Azcoitia, P. Mendez, L.M. Garcia-Segura, Aromatase in the Human Brain, Androg Clin Res Ther. 2 (1) (2021 Dec 1) 189–202.

[8] H. El-Seedi, M. El-Barbary, D. El-Ghorab, L. Bohlin, A.K. Borg-Karlson, U. Goransson, et al., Recent Insights into the Biosynthesis and Biological Activities of Natural Xanthones, Curr Med Chem. 17 (9) (2010 Mar 1) 854–901.

[9] A.I. Shagufta, Recent insight into the biological activities of synthetic xanthone derivatives, Eur J Med Chem. 116 (2016 Jun) 267–280.

[10] L.C. Klein-Júnior, A. Campos, R. Niero, R. Corrèa, Y. Vander Heyden, V.C. Filho, Xanthones and Cancer: from Natural Sources to Mechanisms of Action, Chem Biodivers. (2020). Feb 31;17(2.

[11] M. Pedro, F. Cerqueira, M.E. Sousa, M.S.J. Nascimento, M. Pinto, Xanthones as inhibitors of growth of human cancer cell lines and Their effects on the proliferation of human lymphocytes In Vitro, Bioorg Med Chem. 10 (12) (2002 Dec) 3725–3730.

[12] World Intellectual Property Organization (WIPO) [Internet]. 2020. CN108619132 - Application of 7-nitro-1,3-dihydroxyxanthone in the preparation of anti-tumor drugs.

[13] R. Reitsamer, F. Peintinger, E. Forsthuber, A. Sir, The applicability of Magseed® for targeted axillary dissection in breast cancer patients treated with neoadjuvant chemotherapy, Breast 57 (2021 Jun) 113–117.

[14] Lancet Oncol. 7 (8) (2006 Aug) 633–643.

[15] A.G. Mukherjee, U.R. Wanjari, D. Nagarajan, K. Vibhaa, V. Anagha, P. Joshua Paul, et al., Letrozole: Pharmacology, toxicity and potential therapeutic effects, Life Sci. 310 (2022 Dec) 121074.

[16] A. Robinson, A review of the use of exemestane in early breast cancer, Ther Clin Risk Manag. 5 (1) (2009 Feb) 91–98.

[17] C. Jackson, L. Finikarides, A.L.J. Freeman, The adverse effects of trastuzumab-containing regimes as a therapy in breast cancer: A piggy-back systematic review and meta-analysis, PLoS One 17 (12) (2022 Dec 1) e0275321.

[18] K. Ishii, N. Morii, H. Yamashiro, Pertuzumab in the treatment of HER2-positive breast cancer: an evidence-based review of its safety, efficacy, and place in therapy</p>, Core Evid. 14 (2019 Oct) 51–70.

[19] R.K. Ismail, J. van Breeschoten, M.W.J.M. Wouters, M. van Dartel, S. van der Flier, A.K.L. Reyners, et al., Palbociclib dose reductions and the effect on clinical outcomes in patients with advanced breast cancer, Breast 60 (2021 Dec) 263–271.

[20] J.Y. Jhan, W.E. Wang, S.C. Chu, C.H. Cheng, C.H. Chang, Case Report: Ribociclib-induced phototoxicity presented as dyschromia with subsequent bullae formation, Front Oncol. 24 (2023 Aug) 13.

[21] H.S. Rugo, J. Huober, J.A. García-Sáenz, N. Masuda, J.H. Sohn, V.A.M. Andre, et al., Management of Abemaciclib-Associated Adverse Events in Patients with Hormone Receptor-Positive, Human Epidermal Growth Factor Receptor 2-Negative Advanced Breast Cancer: Safety Analysis of MONARCH 2 and MONARCH 3, Oncologist. 26 (1) (2021 Jan 1) 53–65.

[22] G. Roubaud, M. Özgüroğlu, N. Penel, N. Matsubara, N. Mehra, M.P. Kolinsky, et al., Olaparib tolerability and common adverse-event management in patients with metastatic castration-resistant prostate cancer: Further analyses from the PROfound study, Eur J Cancer. 170 (2022 Jul) 73–84.

[23] J.K. Litton, H.S. Rugo, J. Ettl, S.A. Hurvitz, A. Gonçalves, K.H. Lee, et al., Talazoparib in Patients with Advanced Breast Cancer and a Germline BRCA Mutation, N. Engl. J. Med. 379 (8) (2018 Aug 23) 753–763.

[24] K. Kamińska, A. Cudnoch-Jędrzejewska, A Review on the Neurotoxic Effects of Doxorubicin, Neurotox Res. 41 (5) (2023 Oct 23) 383–397.

[25] G.E. Kim, A.R. Ibrahim, D. Shalatouni, N.H. Abouzeid, F. Othman, Paclitaxel-induced acute myocardial infarction: a case report and literature review, BMC Cardiovasc Disord. 24 (1) (2024 Mar 19) 167.

[26] J. Baker, J. Ajani, F. Scotté, D. Winther, M. Martin, M.S. Aapro, et al., Docetaxel-related side effects and their management, Eur. J. Oncol. Nurs. 13 (1) (2009 Feb) 49–59.

[27] A.R. Ahmed, S.M. Hombal, Cyclophosphamide (Cytoxan). A review on relevant pharmacology and clinical uses, J Am Acad Dermatol. 11 (6) (1984 Dec) 1115–1126.

[28] M.Y. Salem, Atezolizumab Induced Neurotoxicity : A Systematic Review, J Exp Neurol. 5 (3) (2024) 121–140.

[29] P. Kotian, A. Boloor, S. Sreenivasan, Study of Adverse Effect Profile of Parenteral Zoledronic Acid in Female Patients with Osteoporosis, J. Clin. Diagn. Res. 10(1): OC04–6 (2016 Jan).

[30] M.R. McClung, Denosumab for the treatment of osteoporosis, Osteoporos Sarcopenia. 3 (1) (2017 Mar) 8–17.

[31] F. da Silva, P. Santos-Júnior, L. Rocha Silva, L. José Quintans-Júnior, E. Ferreira da Silva-Júnior, Nitro compounds against trypanosomatidae parasites: Heroes or villains? Bioorg Med Chem Lett. 75 (2022 Nov) 128930.

[32] J.Y. Zhang, L.J. Zhao, Y.T. Wang, Synthesis and clinical application of small-molecule drugs approved to treat prostatic cancer, Eur J Med Chem. 262 (2023 Dec) 115925.

[33] Hamano T, Endo Y. Drug discovery in Alzheimer's disease by regulating autophagy. In: Autophagy Dysfunction in Alzheimer's Disease and Dementia. Elsevier; 2022. p. 263–90.

[34] M.R. Junna, B.J. Selim, T.I. Morgenthaler, Medical Sedation and Sleep Apnea, Sleep Med Clin. 8 (1) (2013 Mar) 43–58.

[35] Y. Mukaijo, S. Yokoyama, N. Nishiwaki, Comparison of Substituting Ability of Nitronate versus Enolate for Direct Substitution of a Nitro Group, Molecules 25 (9) (2020 Apr 28) 2048.

[36] S. Noriega, J. Cardoso-Ortiz, A. López-Luna, M.D.R. Cuevas-Flores, J.A. Flores De La Torre, The Diverse Biological Activity of Recently Synthesized Nitro Compounds, Pharmaceuticals. (2022). Jun 5;15(6):717.

[37] C.Y. Lee, C. Anamoah, J. Semenya, K.N. Chapman, A.N. Knoll, H.F. Brinkman, et al., Electronic (donating or withdrawing) effects of ortho-phenolic substituents in dendritic antioxidants, Tetrahedron Lett. 61 (11) (2020 Mar) 151607.

[38] P.K. Grover, G.D. Shah, S.a.R.C. Xanthones, Part IV. A new synthesis of hydroxyxanthones and hydroxybenzophenones, Journal of the Chemical Society (resumed) 3982 (1955).

[39] S. Moreau, S. Varache-Lembège, S. Larrouture, D. Fall, A. Neveu, G. Deffieux, et al., (2-Arylhydrazonomethyl)-substituted xanthones as antimycotics: synthesis and fungistatic activity against Candida species, Eur J Med Chem. 37 (3) (2002 Mar) 237–253.

[40] S. Ramakrishnan, N. Mad Nasir, J. Stanslas, A. Imran Faisal Hamdi, M. A. Mohammad Latif, F.F. Baharuddin, One-pot two-component synthesis of halogenated xanthone, 3-o substituted xanthone, and prenylated xanthone derivatives as aromatase inhibitors, Results Chem. 5 (2023 Jan) 100789.

[41] M. Mondal, V.G. Puranik, N.P. Argade, Facile Synthesis of 1,3,7-Trihydroxyxanthone and Its Regioselective Coupling Reactions with Prenal: Simple and Efficient Access to Osajaxanthone and Nigrolineaxanthone F, J Org Chem. 71 (13) (2006 Jun 1) 4992–4995.

[42] B.D. Zhou, L.L. Zeng, Y.G. Tong, J.Y. Fang, Z.P. Ruan, X.Y. Zeng, et al., Synthesis and antitumor, antityrosinase, and antioxidant activities of xanthone, J Asian Nat Prod Res. 20 (5) (2018 May 4) 467–476.

[43] J.S. Lee, S.D. Warkad, P.B. Shinde, A. Kuwar, S.B. Nimse, A highly selective fluorescent probe for nanomolar detection of ferric ions in the living cells and aqueous media, Arab. J. Chem. 13 (12) (2020 Dec) 8697–8707.

[44] M.Q. Tang, H.F. Zhang, Z.W. Zhu, H.M. Fu, A.M. Wang, H. Li, et al., TiZr-base Bulk Metallic Glass with over 50 mm in Diameter, J Mater Sci Technol. 26 (6) (2010 Jun) 481–486.

[45] N.A. Razak, N. Abu, W.Y. Ho, N.R. Zamberi, S.W. Tan, N.B. Alitheen, et al., Cytotoxicity of eupatorin in MCF-7 and MDA-MB-231 human breast cancer cells via cell cycle arrest, anti-angiogenesis and induction of apoptosis, Sci Rep. 9 (1) (2019 Feb 6) 1514.

[46] Gemcitabine NDA #200795. 2011.

[47] T.L. Riss, R.A. Moravec, Use of Multiple Assay Endpoints to Investigate the Effects of Incubation Time, Dose of Toxin, and Plating Density in Cell-Based Cytotoxicity Assays, Assay Drug Dev Technol. 2 (1) (2004 Feb) 51–62.

[48] G. Indrayanto, G.S. Putra, Suhud F, Application in herbal drug research. In, Validation of in-vitro bioassay methods, 2021, pp. 273–307.

[49] A.M.G. Ang, F.G.E. Reyes, Brine Shrimp Lethality of Atuna racemosa Raf. (Chrysobalanaceae) Fruits Extracted with Varying Acetic Acid Concentrations. Asian J Biol, Life Sci. 8 (1) (2019 May 21) 25–29.

[50] J. Liang, R.L. Lupien, H. Xie, R.S. Vachula, M.A. Stevenson, B.P. Han, et al., Lake ecosystem on the Qinghai–Tibetan Plateau severely altered by climatic warming and human activity, Palaeogeogr Palaeoclimatol Palaeoecol. 576 (2021 Aug) 110509.

[51] S.K. Thiagarajan, K.V. Perumal, N.H. Shafie, K.K.A. Kadir, H. Bahari, in: Anti-Proliferative and Apoptotic Induction Effect of Elateriospermum Extract on Human Lung Cancer Cell Line A549, MDPI, Basel Switzerland, 2020, p. 4.

[52] K V, Arapoc DJ, Adam Z, Razali R, Azuin Suliman N, Abu Bakar NA. Phytochemical Screening, In vitro Antioxidant Activities and Zebrafish Embryotoxicity of Abelmoschus esculentus Extracts. Pharmacognosy Journal. 2022 Jun 30;14(3): 690–701.

[53] D. Ghosh, J. Griswold, M. Erman, W. Pangborn, Structural basis for androgen specificity and oestrogen synthesis in human aromatase, Nature 457 (7226) (2009 Jan 8) 219–223.

[54] G.P. Rosa, A. Palmeira, D.I.S.P. Resende, I.F. Almeida, A. Kane-Pagès, M.C. Barreto, et al., Xanthones for melanogenesis inhibition: Molecular docking and QSAR

studies to understand their anti-tyrosinase activity, Bioorg Med Chem. 29 (2021 Jan) 115873.

[55] O. Trott, A.J. Olson, AutoDock Vina: Improving the speed and accuracy of docking with a new scoring function, efficient optimization, and multithreading, J Comput Chem. 31 (2) (2010 Jan 30) 455–461.

[56] R. Patil, S. Das, A. Stanley, L. Yadav, A. Sudhakar, A.K. Varma, Optimized Hydrophobic Interactions and Hydrogen Bonding at the Target-Ligand Interface Leads the Pathways of Drug-Designing, PLoS One 5 (8) (2010 Aug 16) e12029.

[57] M.D. Hanwell, D.E. Curtis, D.C. Lonie, T. Vandermeersch, E. Zurek, G.R. Hutchison, Avogadro: an advanced semantic chemical editor, visualization, and analysis platform, J Cheminform. 4 (1) (2012 Dec 13) 17.

[58] Z. Sheng, S. Ge, X. Xu, Y. Zhang, P. Wu, K. Zhang, et al., Design, synthesis and evaluation of cinnamic acid ester derivatives as mushroom tyrosinase inhibitors, Medchemcomm. 9 (5) (2018 May 1) 853–861.

[59] M. Al-Nema, A. Gaurav, V.S. Lee, Docking based screening and molecular dynamics simulations to identify potential selective PDE4B inhibitor, Heliyon. 6 (9) (2020 Sep) e04856.

[60] T.L. Riss, R.A. Moravec, A.L. Niles, Cell Viability Assays. (2013).

[61] T. Potipiranun, S. Adisakwattana, W. Worawalai, R. Ramadhan, P. Phuwapraisirisan, Identification of Pinocembrin as an Anti-Glycation Agent and α-Glucosidase Inhibitor from Fingerroot (Boesenbergia rotunda): The Tentative Structure⁻Activity Relationship towards MG-Trapping Activity, Molecules (2018). Dec 19;23(12.

[62] J. Clayden, N. Greeves, S. Warren, Organic Chemistry, 2nd Edition., Oxford University Press, 2012, pp. 489–490.

[63] Apebende CG, idante PS, Magu TO, Asogwa FC, Onyebuenyi IB, Unimuke TO, et al. Density functional theory study of the influence of activating and deactivating groups on Naphthalene. Results Chem. 2022 Jan;4:100669.

[64] Tao XM, Wang J cheng, Wang J bao, Feng Q, Gao S yun, Zhang LR, et al. Enhanced anticancer activity of gemcitabine coupling with conjugated linoleic acid against human breast cancer in vitro and in vivo. European Journal of Pharmaceutics and Biopharmaceutics. 2012 Oct;82(2):401–9.

[65] Xie M, Liu D, Yang Y. Anti-cancer peptides: classification, mechanism of action, reconstruction and modification. Open Biol. 2020 Jul 22;10(7).

[66] T. Shan, Q. Ma, K. Guo, J. Liu, W. Li, F. Wang, et al., Xanthones from Mangosteen Extracts as Natural Chemopreventive Agents: Potential Anticancer Drugs, Curr Mol Med. 11 (8) (2011 Nov 1) 666–677.

[67] C. Wu, An important player in brine shrimp lethality bioassay: The solvent, J Adv Pharm Technol Res. 5 (1) (2014 Jan) 57–58.

[68] B. Meyer, N. Ferrigni, J. Putnam, L. Jacobsen, D. Nichols, J. McLaughlin, Brine Shrimp: A Convenient General Bioassay for Active Plant Constituents, Planta Med. 45 (05) (1982 May 29) 31–34.

[69] A. Modarresi Chahardehi, H. Arsad, V. Lim, Zebrafish as a Successful Animal Model for Screening Toxicity of Medicinal Plants, Plants. 9 (10) (2020 Oct 12) 1345.

[70] G.M. Morris, R. Huey, W. Lindstrom, M.F. Sanner, R.K. Belew, D.S. Goodsell, et al., AutoDock4 and AutoDockTools4: Automated docking with selective receptor flexibility, J Comput Chem. 30 (16) (2009 Dec 27) 2785–2791.

[71] D. Ramírez, J. Caballero, Is It Reliable to Take the Molecular Docking Top Scoring Position as the Best Solution without Considering Available Structural Data? Molecules 23 (5) (2018 Apr 28) 1038.

[72] U. Acar Çevik, B.N. Sağlık, D. Osmaniye, S. Levent, B. Kaya Çavuşoğlu, A. B. Karaduman, et al., Synthesis and docking study of benzimidazole-triazolothiadiazine hybrids as aromatase inhibitors, Arch Pharm (weinheim). 353 (5) (2020 May) e2000008.

[73] F. Lombardo, E. Gifford, M. Shalaeva, In Silico ADME Prediction: Data, Models, Facts and Myths, Mini-Rev. Med. Chem. 3 (8) (2003 Dec 1) 861–875.

[74] S. Soga, H. Shirai, M. Kobori, N. Hirayama, Use of amino acid composition to predict ligand-binding sites, J Chem Inf Model. 47 (2) (2007) 400–406.

[75] J. Wang, G. Krudy, T. Hou, W. Zhang, G. Holland, X. Xu, Development of Reliable Aqueous Solubility Models and Their Application in Druglike Analysis, J Chem Inf Model. 47 (4) (2007 Jul 1) 1395–1404.

[76] J.H. Lin, M. Yamazaki, Role of P-Glycoprotein in Pharmacokinetics, Clin Pharmacokinet. 42 (1) (2003) 59–98.

[77] K. Mortelmans, E. Zeiger, The Ames Salmonella/microsome mutagenicity assay, Mutation Research/fundamental and Molecular Mechanisms of Mutagenesis. 455 (1–2) (2000 Nov) 29–60.

[78] M.C. Sanguinetti, M. Tristani-Firouzi, hERG potassium channels and cardiac arrhythmia, Nature 440 (7083) (2006 Mar 22) 463–469.

[79] Lipinski CA, Lombardo F, Dominy BW, Feeney PJ. Experimental and computational approaches to estimate solubility and permeability in drug discovery and development settings 1PII of original article: S0169-409X(96)00423-1. The article was originally published in Advanced Drug Delivery Reviews 23 (1997) 3–25. 1. Adv Drug Deliv Rev. 2001 Mar;46(1–3):3–26.

[80] D.F. Veber, S.R. Johnson, H.Y. Cheng, B.R. Smith, K.W. Ward, K.D. Kopple, Molecular Properties That Influence the Oral Bioavailability of Drug Candidates, J Med Chem. 45 (12) (2002 Jun 1) 2615–2623.

[81] A.K. Ghose, V.N. Viswanadhan, J.J. Wendoloski, A Knowledge-Based Approach in Designing Combinatorial or Medicinal Chemistry Libraries for Drug Discovery. 1. A Qualitative and Quantitative Characterization of Known Drug Databases, J Comb Chem. 1 (1) (1999 Jan 12) 55–68.

[82] A. Daina, O. Michielin, V. Zoete, SwissADME: a free web tool to evaluate pharmacokinetics, drug-likeness and medicinal chemistry friendliness of small molecules, Sci Rep. 7 (1) (2017 Mar 3) 42717.

[83] M. Shweta, D. Rashmi, In-vitro ADME studies of TUG-891, a GPR-120 inhibitor using Swiss ADME predictor, J. Drug Delivery Therapeutics. 9 (2) (2019) 266–369.